2013 European Control Conference (ECC)
July 17-19, 2013, Zürich, Switzerland.

Robust Fault Detection for Systems with Electronic Induced Delays: Application to the Rendezvous Phase of the MSR Mission

R. Fonod, D. Henry, E. Bornschlegl and C. Charbonnel

Abstract— **Two robust fault detection schemes are presented to detect faults affecting the thrust system of the chaser spacecraft involved in the rendezvous phase of the Mars Sample Return (MSR) mission. The idea of both proposed methods is to transform the unstructured uncertainty caused by the electronic induced delays into unknown inputs and decouple them by means of an eigenstructure assignment (EA) technique. The first method utilizes a Cayley-Hamilton theorem based transformation whereas the second relies on a first-order Padé approximation of the time delay. The performances of the proposed schemes are compared by a sensitivity/robustness analysis campaign of 4240 runs within the "high-fidelity" industrial simulator provided by Thales Alenia Space.**

I. Introduction

The problem of time-delay systems is a research subject in the Fault Detection and Isolation (FDI) community, see the surveys [1]–[4] and the references therein. The major papers in this area deal with networked systems since there may exist (bounded but unknown) delays in communications. Only a limited bibliography exist on the research of model-based fault diagnosis for linear time-delay dynamic systems. For instance, in [5], an unknown input observer (UIO) is designed for Fault Detection (FD) of state-delayed systems with known delays. The well known parity space approach is extended in [6] for fault detection of retarded time-delay systems. In [7], [8], the proposed method aims at formulating the robustness as well as the sensitivity of residual signals to the unknown inputs as well as to the faults in terms of L_2-gain and, based on it, to formulate the design of fault detection filters as an optimization problem. In [9], a robust fault detection and identification approach based on an adaptive observer is developed for uncertain continuous linear time-invariant (LTI) systems with multiple discrete time-delays in both states and outputs. Recently, a geometric approach for FDI of retarded and neutral time-delay systems was developed in [10]. Robust fault detector design for a class of linear systems with some nonlinear perturbations and mixed neutral and discrete time-varying delays is investigated in [11] using a descriptor technique, Lyapunov-Krasovskii functional and a suitable change of variables.

This research work was supported by the European Space Agency (ESA) and Thales Alenia Space in the frame of the ESA Networking/Partnering Initiative (NPI) program

R. Fonod and D. Henry are with University of Bordeaux, IMS-lab, Automatic control group, 351 cours de la libération, 33405 Talence, France. E-mail: {robert.fonod; david.henry}@ims-bordeaux.fr

E. Bornschlegl is with European Space Agency, ESTEC, Keplerlaan 1, 2200 AG Noordwijk, The Netherlands. E-mail: eric.bornschlegl@esa.int

C. Charbonnel is with Thales Alenia Space, 100 Bd du Midi, 06156 Cannes, France. E-mail: catherine.charbonnel@thalesaleniaspace.com

In this paper, two FD schemes are proposed to cope with the issue of robust residual generation for a class of LTI systems with disturbances and input delays. The system is modelled as a continuous-time one with digital control and delayed control input. Such modelling approach was presented in [12]. By introducing a Cayley-Hamilton theorem based and Padé approximation based transformation, influence/uncertainty of the time-varying input delay is transformed into unknown input (UI), which as shown, greatly facilitates the above mentioned difficulty. Finally, the disturbance and the UI vector are lumped and decoupled by means of Eigenstructure Assignment (EA) technique.

These two methods have been successfully demonstrated as applicable for the FD of the Mars Sample Return (MSR) mission with a "high-fidelity" industrial simulator, under realistic conditions, taking into account the effects that the GNC (Guidance, Navigation, Control) unit has on the FD performances. The research work draws expertise from actions undertaken within the European Space Agency, Thales Alenia Space and the IMS laboratory (Univ. Bordeaux 1), which develop a collaborative effort to create new robust on-board FDI technologies that may significantly advance the spacecraft autonomy.

II. Problem Formulation

Consider a continuous LTI system given by

$$\begin{aligned} \dot{\boldsymbol{x}}(t) &= \boldsymbol{A}\boldsymbol{x}(t) + \boldsymbol{B}\boldsymbol{u}(t) + \boldsymbol{E}_f\boldsymbol{f}(t) + \boldsymbol{E}_{d_1}\boldsymbol{d}^1(t) \\ \boldsymbol{y}(t) &= \boldsymbol{C}\boldsymbol{x}(t) \end{aligned} \tag{1}$$

where $\boldsymbol{x}(t) \in \mathbb{R}^n$, $\boldsymbol{u}(t) \in \mathbb{R}^{n_u}$, $\boldsymbol{y}(t) \in \mathbb{R}^{n_y}$ are state, input, and measurement vectors, respectively. $\boldsymbol{d}^1(t) \in \mathbb{R}^{n_d}$ and $\boldsymbol{f}(t) \in \mathbb{R}^{n_f}$ are the unknown disturbance and the fault vector. $\boldsymbol{A}$, $\boldsymbol{B}$, $\boldsymbol{C}$, $\boldsymbol{E}_f$ and $\boldsymbol{E}_{d_1}$ are known matrices of appropriate dimensions. The pair $(\boldsymbol{A}, \boldsymbol{C})$ is assumed to be observable.

Suppose that the system is controlled by a discrete-time controller with the sampling time T and that there exists an upper bounded electronic-induced delay $\tau_k \in \mathbb{R}$ in the actuation system so that the controller signal $\boldsymbol{u}_k^c \in \mathbb{R}^{n_u}$, generated at $t = t_k = kT, k = 1, 2, ...$, arrives at the actuator at time instant $t_k + \tau_k$. Recalling the fact, every control signal $\boldsymbol{u}_k^c$ is held by a zero-order holder and only valid over the interval $[t_k + \tau_k, t_{k+1} + \tau_{k+1})$, we have

$$\boldsymbol{u}(t) = \begin{cases} \boldsymbol{u}_k^c, & \forall t \in [t_k + \tau_k, t_{k+1} + \tau_{k+1}) \\ \boldsymbol{u}_0^c, & \forall t \in [0, \tau_1) \end{cases} \tag{2}$$

The problem addressed in this paper can be formulated as:

Problem 1: Design a discrete-time residual generator $\boldsymbol{r}(z) = \boldsymbol{H}_y(z)\boldsymbol{y}(z) + \boldsymbol{H}_u(z)\boldsymbol{u}(z)$, where $\boldsymbol{H}_y/\boldsymbol{H}_u$ are linear

dynamic filters, so that $\boldsymbol{r}$ is robust against the uncertain time-varying delay τ_k and disturbance vector $\boldsymbol{d}^1$.
To solve Problem 1, the influence of τ_k is transformed to unknown input $\boldsymbol{d}^2$ and together with $\boldsymbol{d}^1$ decoupled by means of EA technique, $\boldsymbol{H}_y/\boldsymbol{H}_u$ being observer-based filters.

III. Transformation into Polytopic Uncertainty

Assume that τ_k can be expressed as: $\tau_k = lT + \delta_k \leq \bar{\tau}$, where l is a known integer, $\bar{\tau}$ is the upper bound of τ_k and $\delta_k \in \mathbb{R}$ is the unknown varying part of τ_k, bounded by $0 \leq \delta_k < mT$, with m being a known integer. In the next, assume that $m = 1$. (The case when $m > 1$, is discussed in [13].)

If we assume that $\boldsymbol{d}^1$ and $\boldsymbol{f}$ are constant during each time interval T, that is a reasonable assumption from a practical point of view, then the discrete representation of (1) is

$$\begin{aligned} \boldsymbol{x}_{k+1} &= \bar{\boldsymbol{A}}\boldsymbol{x}_k + \boldsymbol{\Gamma}_0^{\delta_k}\boldsymbol{u}_{k-l}^c + \boldsymbol{\Gamma}_1^{\delta_k}\boldsymbol{u}_{k-l-1}^c + \bar{\boldsymbol{E}}_f\boldsymbol{f}_k + \bar{\boldsymbol{E}}_{d_1}\boldsymbol{d}_k^1 \\ \bar{\boldsymbol{y}}_k &= \bar{\boldsymbol{C}}\boldsymbol{x}_k \end{aligned} \tag{3}$$

where

$$\bar{\boldsymbol{A}} = e^{\boldsymbol{A}T}, \quad \boldsymbol{\Gamma}_0^{\delta_k} = \int_0^{T-\delta_k} e^{\boldsymbol{A}t}dt\boldsymbol{B}, \quad \bar{\boldsymbol{E}}_{d_1} = \int_0^{T} e^{\boldsymbol{A}t}dt\boldsymbol{E}_{d_1}$$

$$\bar{\boldsymbol{C}} = \boldsymbol{C}, \quad \boldsymbol{\Gamma}_1^{\delta_k} = \int_{T-\delta_k}^{T} e^{\boldsymbol{A}t}dt\boldsymbol{B}, \quad \bar{\boldsymbol{E}}_f = \int_0^{T} e^{\boldsymbol{A}t}dt\boldsymbol{E}_f$$

Let $\bar{\boldsymbol{B}} = \int_0^T e^{\boldsymbol{A}t}dt\boldsymbol{B}$, then it follows:

$$\boldsymbol{\Gamma}_0^{\delta_k} + \boldsymbol{\Gamma}_1^{\delta_k} = \int_0^T e^{\boldsymbol{A}t}dt\boldsymbol{B} = \bar{\boldsymbol{B}} \tag{4}$$

Furthermore, using (3) and (4), and introducing a new augmented state vector $\boldsymbol{z}_k^T = \begin{bmatrix} \boldsymbol{x}_k^T & (\boldsymbol{u}_{k-l-1}^c)^T \end{bmatrix}$ we obtain

$$\begin{aligned} \boldsymbol{z}_{k+1} &= \hat{\boldsymbol{A}}^{\tau_k}\boldsymbol{z}_k + \hat{\boldsymbol{B}}^{\tau_k}\boldsymbol{u}_{k-l}^c + \hat{\boldsymbol{E}}_f\boldsymbol{f}_k + \hat{\boldsymbol{E}}_{d_1}\boldsymbol{d}_k^1 \\ \boldsymbol{y}_k &= \hat{\boldsymbol{C}}\boldsymbol{z}_k \end{aligned} \tag{5}$$

where

$$\hat{\boldsymbol{A}}^{\delta_k} = \begin{bmatrix} \bar{\boldsymbol{A}} & \boldsymbol{\Gamma}_1^{\delta_k} \\ \boldsymbol{0} & \boldsymbol{0} \end{bmatrix}, \quad \hat{\boldsymbol{B}}^{\delta_k} = \begin{bmatrix} \bar{\boldsymbol{B}} - \boldsymbol{\Gamma}_1^{\delta_k} \\ \boldsymbol{I} \end{bmatrix}$$

$$\hat{\boldsymbol{C}} = \begin{bmatrix} \bar{\boldsymbol{C}} & \boldsymbol{0} \\ \boldsymbol{0} & \boldsymbol{I} \end{bmatrix}, \quad \hat{\boldsymbol{E}}_{d_1} = \begin{bmatrix} \bar{\boldsymbol{E}}_{d_1} \\ \boldsymbol{0} \end{bmatrix}, \quad \hat{\boldsymbol{E}}_f = \begin{bmatrix} \bar{\boldsymbol{E}}_f \\ \boldsymbol{0} \end{bmatrix}$$

In this model, $\boldsymbol{\Gamma}_1^{\delta_k}$ is strongly dependent on the uncertain term δ_k. Therefore system (5) is an uncertain time-varying system. The next step is to transform this model to an uncertain polytopic system. This can be done by means of a Cayley-Hamilton theorem based transformation.

A. Expressing the Uncertainty as Polytopes of Matrices

Let us first consider the following theorem (see [14]):

Theorem 1: The characteristic polynomial of matrix $\boldsymbol{A}$ is

$$p(\lambda) = \det(\lambda\boldsymbol{I} - \boldsymbol{A}) = \lambda^n + c_{n-1}\lambda^{n-1} + \ldots + c_1\lambda + c_0 \tag{6}$$

then $e^{\boldsymbol{A}t}$ can be written as

$$e^{\boldsymbol{A}t} = s_1(t)\boldsymbol{I} + s_2(t)\boldsymbol{A} + \ldots + s_n(t)\boldsymbol{A}^{n-1} \tag{7}$$

where $s_i(t)$, $1 \leq i \leq n$ are solutions to the n^{th} order homogenous scalar differential equation

$$s^{(n)}(t) + c_{n-1}s^{(n-1)}(t) + \ldots + c_1 s'(t) + c_0 s(t) = 0 \tag{8}$$

satisfying the following initial conditions

$$s_i^{(i-1)}(0) = 1, \quad s_i^{(j)}(0) = 0 \quad \text{for} \quad j \neq i-1, 0 \leq j \leq n-1$$

Proof: The proof can be found in [14]. ∎

Based on theorem 1, proposition given in [13] is considered:

Proposition 1: The Cayley-Hamilton theorem based transformation of $\boldsymbol{\Gamma}_1^{\delta_k}$ can be expressed as follows

$$\boldsymbol{\Gamma}_1^{\delta_k} = \sum_{i=1}^{2n} \mu_i^k \boldsymbol{U}_i \tag{9}$$

where $\boldsymbol{U}_i$ are constant matrices and $\sum_{i=1}^{2n} \mu_i^k = 1, \mu_i^k > 0$.

Proof: Using (7), we have

$$\boldsymbol{\Gamma}_1^{\delta_k} = \int_{T-\delta_k}^{T} e^{\boldsymbol{A}t}dt\boldsymbol{B} = \sum_{i=1}^{n} \left[\left(\int_{T-\delta_k}^{T} s_i(t)dt \right) \boldsymbol{A}^{i-1}\boldsymbol{B} \right] \tag{10}$$

Define

$$s_i^{\max} = \max_{0 \leq \delta_k \leq T} \int_{T-\delta_k}^{T} s_i(t)dt, \quad i = 1, 2, \ldots, n$$

$$s_i^{\min} = \min_{0 \leq \delta_k \leq T} \int_{T-\delta_k}^{T} s_i(t)dt, \quad i = 1, 2, \ldots, n$$

then (10) can be rewritten as

$$\boldsymbol{\Gamma}_1^{\delta_k} = \sum_{i=1}^{n} \left(\alpha_{i,0}^k s_i^{\min} + \alpha_{i,1}^k s_i^{\max} \right) \boldsymbol{A}^{i-1}\boldsymbol{B} \tag{11}$$

where $\alpha_{i,0}^k$ and $\alpha_{i,1}^k$ are two time-varying unknown parameters satisfying $0 \leq \alpha_{i,0}^k \leq 1$, $0 \leq \alpha_{i,1}^k \leq 1$, and $\alpha_{i,0}^k + \alpha_{i,1}^k = 1$.

It can be verified that $\int_{T-\delta_k}^{T} s_i(t)dt, i = 1, 2, \ldots, n$ are Lipschitz-continuous on $0 \leq \delta_k \leq T$, i.e. they satisfy

$$\left| \int_{T-\delta_k^1}^{T} s_i(t)dt - \int_{T-\delta_k^2}^{T} s_i(t)dt \right| \leq \kappa_i \left| \delta_k^1 - \delta_k^2 \right|$$

$\forall \delta_k^1, \delta_k^2 \in [0, T]$, where $\kappa_i, i = 1, 2, ..., n$ are the Lipschitz constants. Setting $\mu_{2i-1}^k = \alpha_{i,0}^k/n$, $\mu_{2i}^k = \alpha_{i,1}^k/n$, $\boldsymbol{U}_{2i-1} = ns_i^{\min}\boldsymbol{A}^{i-1}\boldsymbol{B}$, $\boldsymbol{U}_{2i} = ns_i^{\max}\boldsymbol{A}^{i-1}\boldsymbol{B}$, then from (10) and (11) proposition 1 yields. ∎

Following proposition 1, it can be seen that the system (5) can be rewritten to a polytopic uncertain system as follows

$$\begin{aligned} \boldsymbol{z}_{k+1} &= \left(\hat{\boldsymbol{A}}_0 + \sum_{i=1}^{2n} \mu_i^k \hat{\boldsymbol{A}}_i \right) \boldsymbol{z}_k + \\ &+ \left(\hat{\boldsymbol{B}}_0 + \sum_{i=1}^{2n} \mu_i^k \hat{\boldsymbol{B}}_i \right) \boldsymbol{u}_{k-l}^c + \hat{\boldsymbol{E}}_f\boldsymbol{f}_k + \hat{\boldsymbol{E}}_{d_1}\boldsymbol{d}_k^1 \\ \boldsymbol{y}_k &= \hat{\boldsymbol{C}}\boldsymbol{z}_k \end{aligned} \tag{12}$$

where

$$\hat{\boldsymbol{A}}_0 = \begin{bmatrix} \bar{\boldsymbol{A}} & \boldsymbol{0} \\ \boldsymbol{0} & \boldsymbol{0} \end{bmatrix}, \quad \hat{\boldsymbol{A}}_i = \begin{bmatrix} \boldsymbol{0} & \boldsymbol{U}_i \\ \boldsymbol{0} & \boldsymbol{0} \end{bmatrix}$$

$$\hat{\boldsymbol{B}}_0 = \begin{bmatrix} \bar{\boldsymbol{B}} \\ \boldsymbol{I} \end{bmatrix}, \qquad \hat{\boldsymbol{B}}_i = \begin{bmatrix} -\boldsymbol{U}_i \\ \boldsymbol{0} \end{bmatrix}$$

and the rest of the parameters are the same with those in (5).

B. Expressing the Polytopic Uncertainty as an UI

The uncertain parts of (12), where $\hat{\boldsymbol{A}}_i$ and $\hat{\boldsymbol{B}}_i$ are known constant matrices, μ_i^k is an unknown time-varying scalar factor, can be approximated by a disturbance term as in [2]

$$\sum_{i=1}^{2n} \mu_i^k \hat{\boldsymbol{A}}_i \boldsymbol{z}_k + \sum_{i=1}^{2n} \mu_i^k \hat{\boldsymbol{B}}_i \boldsymbol{u}_{k-l}^c = \hat{\boldsymbol{E}}_{d_2} \boldsymbol{d}_k^2 \tag{13}$$

where

$$\hat{\boldsymbol{E}}_{d_2} = \left[\hat{\boldsymbol{A}}_1, \ldots, \hat{\boldsymbol{A}}_{2n}, \hat{\boldsymbol{B}}_1, \ldots, \hat{\boldsymbol{B}}_{2n}\right]$$

$$\boldsymbol{d}_k^2 = \left[\mu_1^k \boldsymbol{z}_k, \ \ldots, \mu_{2n}^k \boldsymbol{z}_k, \ \mu_1^k \boldsymbol{u}_{k-l}^c, \ \ldots, \mu_{2n}^k \boldsymbol{u}_{k-l}^c\right]^T$$

Now, the two unknown inputs $\boldsymbol{d}_k^1$ and $\boldsymbol{d}_k^2$ can be lumped together, and defined to be $\boldsymbol{d}_k$. Correspondingly, the UI distribution matrix $\hat{\boldsymbol{E}}_d$. That is

$$\boldsymbol{d}_k = \begin{bmatrix} (\boldsymbol{d}_k^1)^T & (\boldsymbol{d}_k^2)^T \end{bmatrix}^T, \ \hat{\boldsymbol{E}}_d = \begin{bmatrix} \hat{\boldsymbol{E}}_{d_1} & \hat{\boldsymbol{E}}_{d_2} \end{bmatrix} \tag{14}$$

Taking the above notation into account, the design model is expressed in terms of lumped unknown inputs as

$$\begin{aligned} \boldsymbol{z}_{k+1} &= \hat{\boldsymbol{A}}_0 \boldsymbol{z}_k + \hat{\boldsymbol{B}}_0 \boldsymbol{u}_{k-l}^c + \hat{\boldsymbol{E}}_f \boldsymbol{f}_k + \hat{\boldsymbol{E}}_d \boldsymbol{d}_k \\ \boldsymbol{y}_k &= \hat{\boldsymbol{C}} \boldsymbol{z}_k \end{aligned} \tag{15}$$

This model represents the discrete-time model of the original system (1), that takes into account both disturbances $\boldsymbol{d}_k^1$ and uncertainties caused by electronic-induced delays represented as an additional unknown input $\boldsymbol{d}_k^2$.

IV. Padé Approximation

This section addresses another method to model the effect of the time-varying delay τ_k. Only the necessary developments from [15] are recalled here. Let us assume that τ_k can be represented by a time-varying piecewise continuous (continuous from the right) delay $\tau(t) = \tau_k, \forall t \in [t_k, t_{k+1})$. In this sense, the system input (2) is expressed as

$$\boldsymbol{u}(t) = \boldsymbol{u}^c(t - \tau(t)) \tag{16}$$

where $\boldsymbol{u}^c(t) = \boldsymbol{u}_k^c, \forall t \in [t_k, t_{k+1})$ is the control signal.

A first-order Padé approximation of the time-varying delay $\tau(t)$ is given by

$$e^{-\tau(t)s} \doteq \frac{1 - \frac{\tau(t)}{2}s}{1 + \frac{\tau(t)}{2}s} \tag{17}$$

An equivalent state space representation of (17) is thus

$$\begin{aligned} \dot{\boldsymbol{x}}_d(t) &= \boldsymbol{A}_d(t)\boldsymbol{x}_d(t) + \boldsymbol{B}_d \boldsymbol{u}^c(t) \\ \boldsymbol{u}(t) &= \boldsymbol{C}_d(t)\boldsymbol{x}_d(t) + \boldsymbol{D}_d \boldsymbol{u}^c(t) \end{aligned} \tag{18}$$

where $\boldsymbol{x}_d(t) \in \mathbb{R}^{n_u}$ is the delayed state vector and $\boldsymbol{A}_d(t) = -\frac{2}{\tau(t)}\boldsymbol{I}$, $\boldsymbol{B}_d = \boldsymbol{I}$, $\boldsymbol{C}_d(t) = \frac{4}{\tau(t)}\boldsymbol{I}$, $\boldsymbol{D}_d = -\boldsymbol{I}$.

The augmented state-space description of the system (1) and delayed inputs (18) is:

$$\begin{aligned} \dot{\boldsymbol{z}}(t) &= \hat{\boldsymbol{A}}(t)\boldsymbol{z}(t) + \hat{\boldsymbol{B}}_0 \boldsymbol{u}^c(t) + \hat{\boldsymbol{E}}_f \boldsymbol{f}(t) + \hat{\boldsymbol{E}}_{d_1} \boldsymbol{d}^1(t) \\ \boldsymbol{y}(t) &= \hat{\boldsymbol{C}} \boldsymbol{z}(t) \end{aligned} \tag{19}$$

$$\hat{\boldsymbol{A}}(t) = \begin{bmatrix} \boldsymbol{A} & \boldsymbol{B}\boldsymbol{C}_d(t) \\ \boldsymbol{0} & \boldsymbol{A}_d(t) \end{bmatrix}, \ \hat{\boldsymbol{B}}_0 = \begin{bmatrix} \boldsymbol{B}\boldsymbol{D}_d \\ \boldsymbol{B}_d \end{bmatrix}, \ \hat{\boldsymbol{C}} = \begin{bmatrix} \boldsymbol{C} & \boldsymbol{0} \end{bmatrix}$$

$$\boldsymbol{z}(t) = \begin{bmatrix} \boldsymbol{x}(t) \\ \boldsymbol{x}_d(t) \end{bmatrix}, \qquad \hat{\boldsymbol{E}}_f = \begin{bmatrix} \boldsymbol{E}_f \\ \boldsymbol{0} \end{bmatrix}, \ \hat{\boldsymbol{E}}_{d_1} = \begin{bmatrix} \boldsymbol{E}_{d_1} \\ \boldsymbol{0} \end{bmatrix}$$

Using (18), the uncertainty is present only in $\hat{\boldsymbol{A}}(t)$.

A. Expressing the Time-Varying Uncertainty as an UI

To proceed, consider that $\tau(t)$ can be expressed as

$$\tau(t) = \tau_0 + \Delta\tau(t) \ : \ |\Delta\tau(t)| \leq \bar{\varepsilon} \tag{20}$$

where τ_0 is the nominal delay, $\Delta\tau(t)$ is the variation around τ_0, and $\bar{\varepsilon}$ is the upper bound.

Proposition 2: The time-varying matrix $\hat{\boldsymbol{A}}(t)$ can be decomposed in two parts

$$\hat{\boldsymbol{A}}(t) = \hat{\boldsymbol{A}}_0 + \Delta\hat{\boldsymbol{A}}(t) \tag{21}$$

so that $\hat{\boldsymbol{A}}_0$ is a constant matrix, and $\Delta\hat{\boldsymbol{A}}(t)z(t)$ will play the role of an UI. Expression (21) holds with

$$\hat{\boldsymbol{A}}_0 = \begin{bmatrix} \boldsymbol{A} & \boldsymbol{B}\boldsymbol{C}_d^{\tau_0} \\ \boldsymbol{0} & \boldsymbol{A}_d^{\tau_0} \end{bmatrix}, \ \Delta\hat{\boldsymbol{A}}(t) = \begin{bmatrix} \boldsymbol{0} & -\boldsymbol{B}\boldsymbol{C}_d^{\tau_0} \\ \boldsymbol{0} & -\boldsymbol{A}_d^{\tau_0} \end{bmatrix} \Delta\tau^*(t) \tag{22}$$

where $\boldsymbol{A}_d^{\tau_0} = -\frac{2}{\tau_0}\boldsymbol{I}$, $\boldsymbol{C}_d^{\tau_0} = \frac{4}{\tau_0}\boldsymbol{I}$, and $\Delta\tau^*(t) = \frac{\Delta\tau(t)}{\tau_0 + \Delta\tau(t)}$.

Proof: The proof of proposition 2 can be found in [15]. ■

Finally, the time-varying uncertainty is expressed as an unknown input $\boldsymbol{d}^2(t)$, entering (19) through $\hat{\boldsymbol{E}}_{d_2}$, that is

$$\Delta\hat{\boldsymbol{A}}(t)\boldsymbol{z}(t) = \hat{\boldsymbol{E}}_{d_2}\boldsymbol{d}^2(t) \tag{23}$$

$$\hat{\boldsymbol{E}}_{d_2} = \begin{bmatrix} -\boldsymbol{B}\boldsymbol{C}_d^{\tau_0} \\ -\boldsymbol{A}_d^{\tau_0} \end{bmatrix}, \quad \boldsymbol{d}^2(t) = \Delta\tau^*(t)\boldsymbol{x}_d(t)$$

Now, the two unknown inputs $\boldsymbol{d}^1(t)$ and $\boldsymbol{d}^2(t)$ and their distribution matrices $\hat{\boldsymbol{E}}_{d_1}$ and $\hat{\boldsymbol{E}}_{d_2}$ can be lumped together similarly as in (14). The system (19) can be now written as

$$\begin{aligned} \dot{\boldsymbol{z}}(t) &= \hat{\boldsymbol{A}}_0 \boldsymbol{z}(t) + \hat{\boldsymbol{B}}_0 \boldsymbol{u}^c(t) + \hat{\boldsymbol{E}}_f \boldsymbol{f}(t) + \hat{\boldsymbol{E}}_d \boldsymbol{d}(t) \\ \boldsymbol{y}(t) &= \hat{\boldsymbol{C}} \boldsymbol{z}(t) \end{aligned} \tag{24}$$

Note that (24) has the same structure as (15). The only difference is in the way how the time-varying uncertainty is handled in terms of unknown inputs.

V. Design of the Robust Fault Detection Scheme

A residual generator for discrete-time system (15) is presented in the next[1]. The procedure is based on eigenvectors and eigenvalues assignment. This technique is well tackled in the FDI community, see [2]–[4] for more details. In order to avoid duplicating materials, only the main principles are recalled in the following.

Consider the following residual generator based on full-order observer

$$\begin{aligned} \hat{\boldsymbol{z}}_{k+1} &= (\hat{\boldsymbol{A}}_0 - \boldsymbol{L}\hat{\boldsymbol{C}})\hat{\boldsymbol{z}}_k + \hat{\boldsymbol{B}}_0 \boldsymbol{u}_k^c + \boldsymbol{L}\boldsymbol{y}_k \\ \boldsymbol{r}_k &= \boldsymbol{Q}(\boldsymbol{y}_k - \hat{\boldsymbol{C}}\hat{\boldsymbol{z}}_k) \end{aligned} \tag{25}$$

where $\boldsymbol{r}_k \in \mathbb{R}^{n_p}$, $\hat{\boldsymbol{z}}_k \in \mathbb{R}^{n+n_u}$ is the residual and the state estimation vector, respectively. $\boldsymbol{Q}$ is the residual weighting

[1]The same procedure can be applied for the continuous system (24), but the observer eigenvalues will belong to a different set of stable eigenvalues.

matrix of appropriate dimension. The Z-transformed residual response to faults and unknown inputs is

$$\boldsymbol{r}(z) = \boldsymbol{G}_{rf}(z)\boldsymbol{f}(z) + \boldsymbol{G}_{rd}(z)\boldsymbol{d}(z) \tag{26}$$

where $\boldsymbol{G}_{rf}(z)$ and $\boldsymbol{G}_{rd}(z)$ denote the transfers between $\boldsymbol{f}(z)$ and $\boldsymbol{r}(z)$, and $\boldsymbol{d}(z)$ and $\boldsymbol{r}(z)$, respectively.

Once $\hat{\boldsymbol{E}}_d$ is known, the remaining task is to find matrices $\boldsymbol{L}$ and $\boldsymbol{Q}$ to satisfy $\boldsymbol{G}_{rd}(z) = \boldsymbol{0}$. The assignment of the observer (25) eigenvectors and eigenvalues is a direct way to solve this design problem.

Note that, because the EA technique does not consider a sensitivity constraint in the design procedure, the fault sensitivity performance of the proposed FD scheme can only be verified a posteriori. Specially the subspace of considered faults should not intersect the subspace of decoupled disturbances, i.e. $\text{Im}(\hat{\boldsymbol{E}}_f) \not\subset \text{Im}(\hat{\boldsymbol{E}}_d)$, see [2].

For the decision making algorithm, the idea is to test the variance σ^2 of the j^{th} residual signal r_k^j according to the χ^2 statistic given by Lapin [4]:

$$S_k^N := \frac{(N-1)s^2}{\sigma_0^2},\ s^2 = \frac{\sum_{i=k-N}^{k}(r_i^j - \bar{r}_k^j)^2}{N-1} \tag{27}$$

where $\bar{r}_k^j$ is the mean value of $r_i^j, i = k-N, \dots, k$ and σ_0^2 is the variance of r^j in fault free situation. The statistic (27) has the standard χ^2 sampling distribution with the degree of freedom equal to $N-1$. Thus, for a given $\alpha > 0$ (the significance level), the threshold is determined by (using the standard χ^2 distribution table)

$$J_{th} = \chi_\alpha^2,\ prob\{\chi^2 > \chi_\alpha^2\} = \alpha \tag{28}$$

The decision rule is thus

$$S_k^N = \begin{cases} \leq J_{th},\ H_0\ (\sigma^2 \leq \sigma_0^2) \text{ is accepted} \\ > J_{th},\ H_1\ (\sigma^2 > \sigma_0^2) \text{ is accepted} \end{cases} \tag{29}$$

For the given constant $\alpha > 0$, the change in variance can be detected with a false alarm rate smaller than α.

VI. Application to the MSR Mission

The MSR mission is a future exploration mission undertaken jointly by NASA and ESA. The goal is to return samples from Mars atmosphere and ground to Earth for analysis. It is obvious that the rendezvous phase of this mission can be in danger if a fault occurs in the chaser's systems since the GNC system may not compensate, for example, J_2 disturbances and/or may lose the attitude and/or the position of the sample container. This problem becomes specially critical during the last 20 meters of the rendezvous phase, since the chaser must be correctly positioned in the rendezvous corridor in order to successfully capture the sample container. This motivates ESA to manage studies for the development of on-board FDI solutions. The robust FD schemes presented in the previous sections are potential candidates since one of the critical system in the chaser's actuation system is the thruster modulator unit (TMU), an electronic device with an unknown (but bounded) time-varying delay that manage the actuators (thrusters) used for the control of both the position and the attitude of the chaser spacecraft during the rendezvous phase.

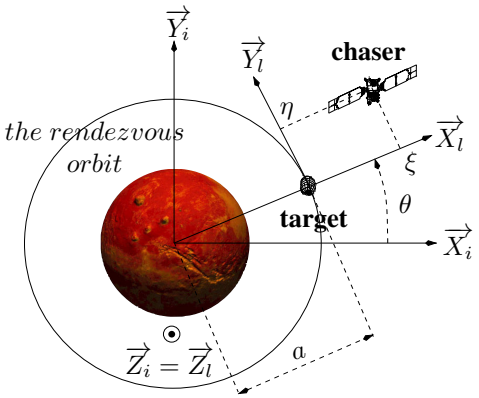

Fig. 1. The Mars rendezvous orbit and the associated frames

A. Modeling the Chaser's Dynamics During the Rendezvous

From [16], [17] we only consider the modeling of the relative position of two spacecrafts on a circular orbit around the planet. The motion of the chaser is derived from the 2nd Newton law. To proceed, let a, m, $\mathcal{G}$ and m_M denote the orbit of the target, the mass of the chaser, the gravitational constant and the mass of the planet Mars. Then, the orbit of the rendezvous being circular, the velocity of any object (e.g. the chaser and the target) is given by the relation $\sqrt{\frac{\mu}{a}}$, where $\mu = \mathcal{G}.m_M$. Let $\mathcal{R}_l : (O_{tgt}, \overrightarrow{X_l}, \overrightarrow{Y_l}, \overrightarrow{Z_l})$ be the frame attached to the target and oriented as shown in Fig. 1. Because the linear velocity of the target is given by the relation $a\dot{\theta}$ in the inertial frame $\mathcal{R}_i : (O_M, \overrightarrow{X_i}, \overrightarrow{Y_i}, \overrightarrow{Y_i})$ (see Fig. 1), it follows:

$$a.\dot{\theta} = \sqrt{\frac{\mu}{a}} \Rightarrow n = \sqrt{\frac{\mu}{a^3}} \tag{30}$$

The chaser motion is due to the following four forces:

- the Mars attraction force $\overrightarrow{F_a}$ given in $\mathcal{R}_l$ by:

$$\overrightarrow{F_a} = -m\frac{\mu}{((a+\xi)^2+\eta^2+\zeta^2)^{3/2}}\left((a+\xi)\overrightarrow{X_l} + \eta\overrightarrow{Y_l} + \zeta\overrightarrow{Z_l}\right);$$

- the centripetal force $\overrightarrow{F_e} = m\left(n^2\xi\overrightarrow{X_l} + n^2\eta\overrightarrow{Y_l} + 0\overrightarrow{Z_l}\right)$;
- the Coriolis force $\overrightarrow{F_c}$ in $\mathcal{R}_l$ is given by:

$$\overrightarrow{F_c} = m\left(2n\dot{\eta}\overrightarrow{X_l} - 2n\dot{\xi}\overrightarrow{Y_l} + 0\overrightarrow{Z_l}\right);$$

- and the forces due to the thrusters:

$$\overrightarrow{F_{thr}} = F_\xi\overrightarrow{X_l} + F_\eta\overrightarrow{Y_l} + F_\zeta\overrightarrow{Z_l}.$$

Then, from the 2nd Newton law, it follows

$$\begin{aligned} \ddot{\xi} &= n^2(a+\xi) + 2n\dot{\eta} - \frac{\mu}{((a+\xi)^2+\eta^2+\zeta^2)^{3/2}}(a+\xi) + \frac{F_\xi}{m} \\ \ddot{\eta} &= n^2\eta - 2n\dot{\xi} - \frac{\mu}{((a+\xi)^2+\eta^2+\zeta^2)^{3/2}}\eta + \frac{F_\eta}{m} \\ \ddot{\zeta} &= -\frac{\mu}{((a+\xi)^2+\eta^2+\zeta^2)^{3/2}}\zeta + \frac{F_\zeta}{m} \end{aligned} \tag{31}$$

where ξ, η, ζ denote the three dimensional position of the chaser (assumed to be a punctual mass) in $\mathcal{R}_l$.

Because the distance between the target and the chaser is smaller than the orbit a, it is possible to derive the

so called Hill-Clohessy-Wiltshire equations from (31) by means of a first order approximation. This boils down to a linear six order state space model with input vector $\boldsymbol{u}(t) = (F_\xi \ F_\eta \ F_\zeta)^T$, output vector $\boldsymbol{y}(t) = (\xi \ \eta \ \zeta)^T$ and state vector $\boldsymbol{x}(t) = (\xi \ \eta \ \zeta \ \dot{\xi} \ \dot{\eta} \ \dot{\zeta})^T$, i.e. from (31) it follows

$$\begin{aligned}\dot{\boldsymbol{x}}(t) &= \boldsymbol{A}\boldsymbol{x}(t) + \boldsymbol{B}\boldsymbol{R}(\hat{Q}_{tgt}(t), \hat{Q}_{chs}(t))\boldsymbol{M}\boldsymbol{u}^{thr}(t) + \boldsymbol{E}_w\boldsymbol{w}(t)\\ \boldsymbol{y}(t) &= \boldsymbol{C}\boldsymbol{x}(t) + \boldsymbol{v}(t)\end{aligned}$$

where $\hat{Q}_{tgt}(t) \in \mathbb{R}^4$ and $\hat{Q}_{chs}(t) \in \mathbb{R}^4$ denote the attitude's quaternion of the target and the chaser, respectively. These quaternions are estimates from the navigation module (NAV). $\boldsymbol{M} \in \mathbb{R}^{3\times 8}$ refers to the thruster configuration matrix, $\boldsymbol{u}^{thr}(t) \in \mathbb{R}^8$ are the thruster inputs. The relative position $\boldsymbol{y}(t) \in \mathbb{R}^3$ is measured by means of a LIDAR unit that is corrupted by a measurement noise $\boldsymbol{v}(t) \in \mathbb{R}^3$, $\boldsymbol{w}(t) \in \mathbb{R}^3$ refers to orbital disturbances entering the system through $\boldsymbol{E}_w$ matrix. The quaternion dependent rotation matrix $\boldsymbol{R}(\cdot)$ performs the projection of the three-dimensional thrust force vector from the chaser's frame on to the target frame $\mathcal{R}_l$.

The considered thrusters faults can be modeled in a multiplicative form according to

$$\boldsymbol{u}_f^{thr}(t) = (\boldsymbol{I}_8 - \boldsymbol{\Psi}(t))\boldsymbol{u}^{thr}(t) \tag{32}$$

where $\boldsymbol{\Psi}(t) = diag\{\psi_i(t)\} : 0 \leq \psi_i(t) \leq 1, \ \ i = 1, \ldots, 8$ models thruster faults, e.g. a locked-in-placed fault can be modeled by $\Psi_i(t) = 1 - \frac{c}{\boldsymbol{u}^{thr_i}(t)}$ where c denotes a constant value (the particular values $c = \{1, 0\}$ allows to consider open/closed faults) whereas a fix value of $\Psi_i(t)$ models a loss of efficiency of the i^{th} thruster. $\boldsymbol{\Psi}(t) = 0 \ \forall t$ means that no fault occurs in the thrusters.

Taking into account some unknown but bounded delays induced by the electronic devices, and uncertainties on the thruster rise times due to the TMU that is modeled here as an unknown time-varying delay $\tau(t) = \tau_0 + \Delta\tau(t)$ with a (constant) nominal delay τ_0 and upper bounded variation part $|\Delta\tau(t)| \leq \bar{\varepsilon}$, the overall model of the chaser dynamics that takes into account both the attitude $\big(Q_{chs}(t)\big)$ and the relative position $(\xi \ \eta \ \zeta)$ of the chaser and target can be written as

$$\begin{aligned}\dot{\boldsymbol{x}}(t) &= \boldsymbol{A}\boldsymbol{x}(t) + \boldsymbol{B}\boldsymbol{u}(t - \tau(t)) + \boldsymbol{E}_f\boldsymbol{f}(t) + \boldsymbol{E}_w\boldsymbol{w}(t)\\ \boldsymbol{y}(t) &= \boldsymbol{C}\boldsymbol{x}(t) + \boldsymbol{v}(t)\end{aligned} \tag{33}$$

by considering $\boldsymbol{R}(\hat{Q}_{tgt}(t), \hat{Q}_{chs}(t))\boldsymbol{M}\boldsymbol{u}^{thr}(t)$ as the delayed input vector $\boldsymbol{u}(t - \tau(t))$ and approximating the fault model $-\boldsymbol{R}(\hat{Q}_{tgt}(t), \hat{Q}_{chs}(t))\boldsymbol{M}\boldsymbol{\Psi}(t)\boldsymbol{u}^{thr}(t)$ in terms of additive faults $\boldsymbol{f}(t) \in \mathbb{R}^3$ acting on the state via a constant distribution matrix $\boldsymbol{E}_f$ (then $\boldsymbol{E}_f = \boldsymbol{B}$).

B. Design of the Fault Detection Schemes

Both schemes use the above derived model (33) to construct the residual generator (25). The uncertainty $\tau(t)$ is handled as an UI entering the augmented system's dynamics, (15) resp. (24), through the distribution matrix $\hat{\boldsymbol{E}}_{d_2}$. The difference between the two proposed methods rest in the different way of treating the uncertainty. The sampling period of the NAV is $T = 0.1s$ and a reasonable value of τ_0 was determined to be exactly one sampling period for the input vector $\boldsymbol{u}$, i.e. $\tau_0 = 0.1$. Since the orbital disturbances $\boldsymbol{w}$ have the same directional properties as the faults ($\boldsymbol{E}_w = \boldsymbol{E}_f$), the residual $\boldsymbol{r}_k$ cannot be decoupled from $\boldsymbol{w}$, thus the disturbance decoupling is not considered here, i.e. $\hat{\boldsymbol{E}}_d = \hat{\boldsymbol{E}}_{d_2}$.

- **Method 1:** first, the model (33) is transformed into the discrete form (15), with $l = 1$ and $m = 1$. It practically means that the unknown delay $\tau(t)$ is assumed to be in the closed interval $[T, 2T)$. The obtained distribution matrix $\hat{\boldsymbol{E}}_d$ has rank($\hat{\boldsymbol{E}}_d$) $= 6$ and a large number of columns. Thus, a full column rank factorization is performed using SVD decomposition. Finally, the obtained distribution matrix is used in the residual generator (25) design using the left EA technique.
- **Method 2:** is formulated using a first order Padé approximation of the input delay. The distribution matrix $\hat{\boldsymbol{E}}_d$ is computed as in (23), with $\tau_0 = 0.1s$. That basically means, that after UI decoupling is achieved, the resulted residual generator (25), using this method, is robust against the time variations $\Delta\tau(t)$ (uncertainty) around the nominal delay τ_0. Finally, the residual generator (25) is converted to discrete-time ($t = kT$) using a Tustin approximation

For both methods, the weighting matrix was determined to be $\boldsymbol{Q} = \boldsymbol{I}_3$, thus $n_p = 3$ and $\boldsymbol{r} = (r^1, r^2, r^3)^T$. The decision rule was computed according to (29) with $N = 10$, $j = 3$ for the first, and $j = 1$ for the second method, respectively. The probability of a false alarm has been fixed at 1% ($\alpha = 0.01$).

Remark 1: In order to compare the proposed approaches, the assigned eigenvalues (dynamics) for Method 2 were chosen to be close to ≈ -0.5, and after the discretization of the continuous residual generator, the obtained closed-loop eigenvalues were used for Method 1.

C. Simulation Results

The aforementioned FD schemes were implemented within the MSR "high-fidelity" industrial simulator provided by Thales Alenia Space. All simulations are carried out under realistic conditions, i.e. the NAV is considered to deliver "non-perfect" measurements. We assume delays induced by the TMU, orbital disturbances (i.e. solar radiation pressure, gravity gradient, atmospheric drag) and uncertainties.

To evaluate the performances in terms of detection time delays (t_d), non-detection ($\hat{P}_{nd}$) and false alarm ($\hat{P}_f$) rates, a sensitivity/robustness analysis campaign of 4240 runs has been performed considering all the aforementioned sources of disturbances, noises, delays and uncertainties whose considered variations range are 10% of the chaser inertia and 5% of the chaser mass. The min. detectable leakage size ($\hat{m}_{leak}$) and min. detectable thrust loss size ($\hat{m}_{loss}$) are also considered as performance criteria. In this study, following fault scenarios were generated on the eight (Thr.No.) thrusters:

- **Case 1:** single thruster opening at 100%
- **Case 2:** thruster closing itself (locked-closed)
- **Case 3:** propellant leakage between 15% and 35%
- **Case 4:** loss of efficiency ranging from 40% to 90%

For each simulation, the fault occurs at $t = 1100s$ and is maintained. The results shown in Tab. I illustrate the

TABLE I

PERFORMANCES OF THE FAULT DETECTION SCHEMES BASED ON 4,240 RUNS

		Method 1								Method 2							
	Thr.No.	**1**	**2**	**3**	**4**	**5**	**6**	**7**	**8**	**1**	**2**	**3**	**4**	**5**	**6**	**7**	**8**
Case 1	$min(t_d)\ [s]$	1	1.1	1	1.1	1.1	0.9	1.1	0.9	0.6	0.6	0.6	0.6	0.6	0.6	0.6	0.6
	$max(t_d)\ [s]$	1	1.1	1	1.1	1.1	1	1.1	1	0.7	0.7	0.6	0.6	0.7	0.7	0.7	0.7
	$med(t_d)\ [s]$	1	1.1	1	1.1	1.1	1	1.1	1	0.7	0.7	0.6	0.6	0.6	0.6	0.6	0.6
Case 2	$min(t_d)\ [s]$	8.7	13.5	9.7	5	25.1	17.6	12.2	7.7	10.3	10.4	8.7	7.7	17.4	13.5	7	8.9
	$max(t_d)\ [s]$	12.5	18.2	11.3	16.4	33.9	25.3	14.1	14.8	12.1	12.2	10.2	10	23.8	21.8	10.5	13.3
	$med(t_d)\ [s]$	10.8	14.8	10.4	15.1	28.8	22.7	13	12.4	11.1	11.3	9.3	9.1	20.7	17.7	8.8	11.1
Case 3	$min(t_d)\ [s]$	1.4	1.5	1.4	1.6	1.6	1.4	1.6	1.3	1	1	0.9	0.9	0.9	0.9	0.9	0.9
	$max(t_d)\ [s]$	2.7	2.6	2.8	2.6	2.8	2.6	2.8	2.5	1.8	1.8	2.0	1.9	2.3	2.3	2.1	1.9
	$med(t_d)\ [s]$	1.7	1.8	1.7	1.8	1.9	1.6	1.9	1.6	1.2	1.2	1.1	1.1	1.1	1.1	1.1	1.1
	$\hat{m}_{leak}\ [\%]$	15	15	15	15	15	15	15	15	20	20	15	15	15	20	20	20
	$\hat{P}_{nd}$	0	0	0	0	0	0	0	0	0.2	0.2	0	0	0	0.01	0.17	0.19
Case 4	$min(t_d)\ [s]$	9.4	13.5	9.7	5	25.1	17.6	12.2	7.9	10.3	10.4	8.6	7.7	17.4	13.5	7	9.6
	$max(t_d)\ [s]$	53.9	100	85.1	43.2	97.7	98.9	77.6	77.7	49.4	35.9	36.2	36	31.2	79.3	51.6	54.6
	$med(t_d)\ [s]$	11.4	15.6	11	15.35	29.4	24.6	13.3	12.9	11.7	12.1	10	9.7	21.4	18.25	9.7	11.9
	$\hat{m}_{loss}\ [\%]$	50	60	60	60	70	60	60	60	50	40	40	40	50	50	40	40
	$\hat{P}_{nd}$	0.15	0.31	0.18	0.29	0.37	0.22	0.31	0.16	0	0	0	0	0.17	0.14	0	0

effectiveness and good reliability characteristics of the proposed methods since no false alarms have been revealed, i.e. $\hat{P}_f = 0$ for all fault cases, thrusters and for both methods. Further, $\hat{P}_{nd} = 0$ was observed for case 1 and case 2, again for all thrusters and both methods (these results are omitted from Tab. I due to space limitations). It can be seen that the second method presents a greater sensitivity level to the leakage type faults (see Fig. 2 for illustration) as well as handles the other fault types better.

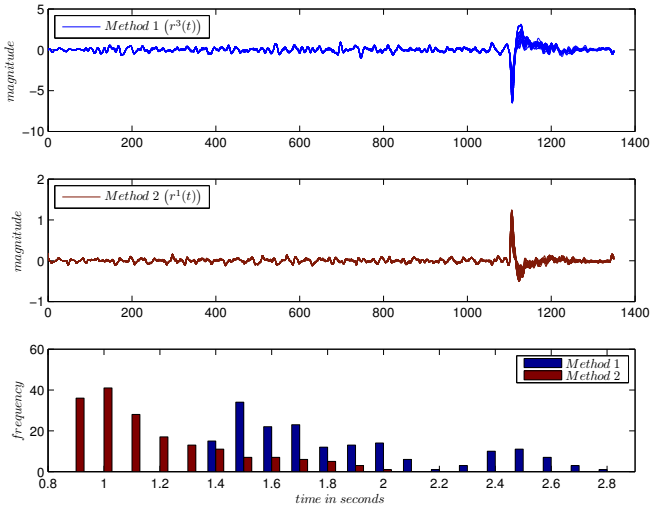

Fig. 2. Residual signals and the corresponding histogram of the detection time t_d for the leakage type of fault affecting the 3rd thruster

VII. CONCLUSIONS

In this paper, two residual-based FD schemes were proposed that are robust against unknown time-varying delays induced by electronic devices. The idea is to transform the unstructured uncertainty to unknown input and decouple it by means of an EA technique. The first method utilizes a Cayley-Hamilton theorem based transformation whereas the second method relies on a first-order Padé approximation. Simulation results show that all considered fault scenarios are covered with the suggested FD schemes. Some performance indicators allows to demonstrate (in a statistical point of view) the reliability (no false alarm) and the efficiency (reasonable detection time) of the proposed schemes.

REFERENCES

[1] R. S. Mangoubi, *Robust estimation and failure detection: A concise treatment*. Springer Verlag New York, Inc., 1998.

[2] J. Chen and R. Patton, *Robust model-based fault diagnosis for dynamic systems*. Kluwer Academic Publishers, 1999.

[3] M. Blanke, M. Kinnaert, J. Lunze, and M. Staroswiecki, *Diagnosis and Fault-Tolerant Control*. Springer Verlag, 2006.

[4] S. Ding, *Model-based fault diagnosis techniques: design schemes, algorithms, and tools*. Springer Verlag, 2008.

[5] H. Yang and M. Saif, "Observer design and fault diagnosis for state-retarded dynamical systems," *Automatica*, vol. 34, no. 2, pp. 217–227, 1998.

[6] F. Kratz, W. Nuninger, and S. Ploix, "Fault detection for time-delay systems: A parity space approach," in *American control conference*, 1998, pp. 2009–2011.

[7] B. Jiang, M. Staroswiecki, and V. Cocquempot, "H_∞ fault detection filter design for linear discrete-time systems with multiple time delays," *International Journal of System Science*, vol. 34, no. 5, pp. 365–373, 2003.

[8] B. Leishi, T. Zuohua, and S. Songjiao, "RFDF design for linear time-delay systems with unknown inputs and parameter uncertainties," *International Journal of System Science*, vol. 38, no. 2, pp. 139–149.

[9] C. Jiang and D. Zhou, "Fault detection and identification for uncertain linear time-delay systems," *Computers and Chemical Engineering*, vol. 30, no. 2, pp. 228–242, 2005.

[10] N. Meskin and K. Khorasani, "Robust fault detection and isolation of time-delay systems using a geometric approach," *Automatica*, vol. 45, no. 6, pp. 1567 – 1573, 2009.

[11] H. Karimi, M. Zapateiro, and N. Luo, "A linear matrix inequality approach to robust fault detection filter design of linear systems with mixed time-varying delays and nonlinear perturbations," *Journal of the Franklin Institute*, vol. 347, no. 6, pp. 957–973, 2010.

[12] Y. Mikheev, V. Sobolev, and E. Fridman, "Asymptotic analysis of digital control systems," *Automation and Remote Control*, vol. 49, no. 9, pp. 1175–1180, 1988.

[13] Y. Wang, S. Ding, H. Ye, and G. Wang, "A new fault detection scheme for networked control systems subject to uncertain time-varying delay," *IEEE Transactions on Signal Processing*, vol. 56, no. 10, 2008.

[14] I. Leonard, "The matrix exponential," *SIAM review*, vol. 38, no. 3, pp. 507–512, 1996.

[15] R. Fonod, D. Henry, C. Charbonnel, and E. Bornschlegl, "Robust thruster fault diagnosis: Application to the rendezvous phase of the mars sample return mission," in *2nd CEAS Specialist Conference on Guidance, Navigation & Control*, Delft, The Netherlands, 2013.

[16] B. Wie, *Space vehicle dynamics and control*. AIAA, 1998.

[17] M. J. Sidi, *Spacecraft dynamics and control: a practical engineering approach*. Cambridge university press, 2000, vol. 7.